

LA-UR-21-31455

Accepted Manuscript

Heterogeneous isotope effects decouple conifer leaf and branch sugar ^{18}O and ^{13}C

Fiorella, Richard Pascal

Kannenberg, Steven A

Anderegg, William R L

Monson, Russell K.

Ehleringer, James R

Provided by the author(s) and the Los Alamos National Laboratory (2022-04-14).

To be published in: Oecologia

DOI to publisher's version: 10.1007/s00442-022-05121-y

Permalink to record:

<http://permalink.lanl.gov/object/view?what=info:lanl-repo/lareport/LA-UR-21-31455>



Los Alamos National Laboratory, an affirmative action/equal opportunity employer, is operated by Triad National Security, LLC for the National Nuclear Security Administration of U.S. Department of Energy under contract 89233218CNA000001. By approving this article, the publisher recognizes that the U.S. Government retains nonexclusive, royalty-free license to publish or reproduce the published form of this contribution, or to allow others to do so, for U.S. Government purposes. Los Alamos National Laboratory requests that the publisher identify this article as work performed under the auspices of the U.S. Department of Energy. Los Alamos National Laboratory strongly supports academic freedom and a researcher's right to publish; as an institution, however, the Laboratory does not endorse the viewpoint of a publication or guarantee its technical correctness.

[Click here to view linked References](#)

Heterogeneous isotope effects decouple conifer leaf and branch sugar $\delta^{18}\text{O}$ and $\delta^{13}\text{C}$

Richard P. Fiorella^{1,2,†,*}, Steven A. Kannenberg³, William R. L. Anderegg^{2,3}, Russell K. Monson^{4,5}, James R. Ehleringer^{2,3}

1: Department of Geology and Geophysics, University of Utah, Salt Lake City, UT 84112

2: Global Change and Sustainability Center, University of Utah, Salt Lake City, UT 84112

3: School of Biological Sciences, University of Utah, Salt Lake City, UT 84112

4: Department of Ecology and Evolutionary Biology, University of Arizona, Tucson, AZ 85721

5: Laboratory of Tree Ring Research, University of Arizona, Tucson, AZ 85721

†: Present address: Earth and Environmental Sciences Division, Los Alamos National Laboratory, Los Alamos, NM 87545

Author ORCIDs

Rich Fiorella: 0000-0002-0824-4777

Steve Kannenberg: 0000-0002-4097-9140

Bill Anderegg: 0000-0001-6551-3331

Russell Monson: 0000-0002-7671-4371

Jim Ehleringer: 0000-0003-2050-3636

*Corresponding author: Richard P. Fiorella

Address: Earth and Environmental Sciences Division, Los Alamos National Laboratory, Los Alamos NM 87545; Email address: rfiorella@lanl.gov; Phone number: (385)-202-3760

Author Contributions: All authors contributed to the planning and design of the research, contributed to interpretation of the data, and wrote the manuscript. RPF and SAK conducted fieldwork and collected the samples, RPF performed the sample preparation and analysis and wrote the initial draft of the manuscript.

1 **Abstract**

2 Isotope ratios of tree-ring cellulose are a prominent tool to reconstruct paleoclimate and plant
3 responses to environmental variation. Current models for cellulose isotope ratios assume a
4 transfer of the environmental signals recorded in bulk leaf water to carbohydrates and ultimately
5 into stem cellulose. However, the isotopic signal of carbohydrates exported from leaf to branch
6 may deviate from mean leaf values if spatial heterogeneity in isotope ratios exists in the leaf. We
7 tested whether the isotopic heterogeneity previously observed along the length of a ponderosa
8 pine (*Pinus ponderosa*) leaf water was preserved in photosynthetic products. We observed an
9 increase in both sugar and bulk tissue $\delta^{18}\text{O}$ values along the needle, but the increase in
10 carbohydrate $\delta^{18}\text{O}$ values was dampened relative to the trend observed in leaf water. In contrast,
11 $\delta^{13}\text{C}$ values of both sugar and bulk organic matter were invariant along the needle. Phloem-
12 exported sugar measured in the branch below the needles did not match whole-needle values of
13 $\delta^{18}\text{O}$ or $\delta^{13}\text{C}$. Instead, there was a near-constant offset observed between branch and needle sugar
14 $\delta^{13}\text{C}$ values, while branch $\delta^{18}\text{O}$ values were most similar to $\delta^{18}\text{O}$ values observed for sugar at the
15 base of the needle. The observed offset between branch and needle sugar $\delta^{18}\text{O}$ values likely
16 arises from partial isotope oxygen exchange between sugars and water during phloem loading
17 and transport. An improved understanding of the conditions producing differential $\delta^{13}\text{C}$ and $\delta^{18}\text{O}$
18 isotope effects between branch phloem and needle sugars could improve tree-ring-based climate
19 reconstructions.

20

21 **Keywords:** cellulose, ponderosa pine, stable isotopes, sugars, tree rings

22

23

24 **Introduction**

25 Tree-ring archives have been widely used to reconstruct ecosystem responses to
26 environmental extremes such as drought, and to reconstruct past climate and fire regimes
27 (D'Arrigo et al. 2001; Cook et al. 2010; Babst et al. 2014; Williams et al. 2020). While initial
28 studies on tree-ring archives focused on physical properties of the wood, such as ring widths or
29 density, carbon and oxygen isotope ratios in tree-ring cellulose provide additional process-level
30 information (McCarroll and Loader 2004; Gessler et al. 2014). Tree-ring oxygen isotope ratios
31 have been used to reconstruct climate variables such as temperature, precipitation, or vapor
32 pressure deficit (e.g., Libby et al. 1976; Danis et al. 2006; Treydte et al. 2006; Roden and
33 Ehleringer 2007; Sidorova et al. 2009; Kahmen et al. 2011), while tree-ring carbon isotope ratios
34 have been used to reconstruct variations in intrinsic water use efficiency (e.g., Saurer et al. 2014;
35 Frank et al. 2015; Mathias and Thomas 2021). The wide range of applications for stable isotope
36 ratios of tree rings has motivated substantial interest in their use, but their utility can be expanded
37 through a more comprehensive knowledge of the environmental factors that drive spatial and
38 temporal variability (Reynolds-Henne et al. 2007; Gessler et al. 2013; Treydte et al. 2014;
39 Cheesman and Cernusak 2016).

40 Models of tree ring-climate interactions predict how isotope ratios track environmental
41 signals from leaf water to tree-ring cellulose (Farquhar et al. 1989; Saurer et al. 1997; Roden et
42 al. 2000; Barbour and Farquhar 2000; Gessler et al. 2014), with the carbon isotope ratios of C₃
43 photosynthetic products varying in response to changes in the ratio of the atmosphere-to-leaf
44 CO₂ mole fraction (e.g., Farquhar et al. 1989). Prior studies tracing the isotopic signal of recent
45 photosynthates to tree-ring cellulose have noted that variations in leaf-level $\delta^{13}\text{C}$ are often
46 attenuated, perhaps associated with mixing between photosynthates of different ages (Brandes et

47 al. 2006; Gessler et al. 2009; Offermann et al. 2011). Moreover, $\delta^{13}\text{C}$ values of sugars exported
48 from the leaves that are used in tree-ring cellulose construction may be offset from their initial
49 values as a result of post-photosynthetic fractionation associated with processes, such as
50 construction and breakdown of transitory starch (Brandes et al. 2006; Gessler et al. 2008), lignin
51 and lipid metabolism (Benner et al. 1987; Hobbie and Werner 2004), respiration and bark
52 photosynthesis (Cernusak and Marshall 2000; Cernusak et al. 2001), and phloem loading and
53 mixing (Offermann et al. 2011; Gessler et al. 2014; Bögelein et al. 2019).

54 In contrast, the oxygen isotope ratio of leaf sugars is primarily determined by the $\delta^{18}\text{O}$
55 values of the leaf water with an offset of $\sim 27\text{‰}$ (Sternberg et al. 1986; Cernusak et al. 2003;
56 Lehmann et al. 2017). When these sugars are used to build cellulose, a fraction of their oxygen
57 atoms will exchange with the surrounding xylem water. The extent of exchange is thought to be
58 controlled by the fraction of sugars that cycle between hexoses and trioses prior to incorporation
59 into cellulose (Hill et al. 1995; Barbour and Farquhar 2000; Cheesman and Cernusak 2016).
60 These fractionation and exchange processes are commonly modeled using an empirical formula
61 relating the enrichment of ^{18}O above source water ($\Delta^{18}\text{O}_x =$
62 $(\delta^{18}\text{O}_x - \delta^{18}\text{O}_{source}) / (1 + \delta^{18}\text{O}_{source} / 1000)$) between leaf water ($\Delta^{18}\text{O}_L$) and plant cellulose
63 ($\Delta^{18}\text{O}_{cellulose}$) (e.g., Barbour 2007):

$$64 \quad \Delta^{18}\text{O}_{cellulose} = \Delta^{18}\text{O}_L(1 - p_{ex}p_x) + \varepsilon_{wc}$$

65 where p_{ex} is the fraction of oxygen atoms in sugars that exchange with local water, p_x is the
66 proportion of local water that has not been evaporatively enriched, and ε_{wc} is the oxygen isotope
67 fractionation during cellulose biosynthesis. The $p_{ex}p_x$ term is a ‘damping factor,’ and reflects the
68 exchange process that prevents full expression of $\Delta^{18}\text{O}_L$ variability in cellulose (Cheesman and
69 Cernusak 2016).

70 An implied assumption in these models is that leaf-exported assimilates reflect the mean
71 $\delta^{18}\text{O}$ values measured in leaf water. However, progressive enrichment of heavy water
72 isotopologues—or the tendency of $\delta^{18}\text{O}$ to increase along the leaf and away from veins—has been
73 described many angiosperm and gymnosperm species (Helliker and Ehleringer 2000; Farquhar
74 and Gan 2003; Šantrůček et al. 2007; English et al. 2007), including pines (Shu et al. 2008;
75 Kannenberg et al. 2021). These leaf water isotope ratio heterogeneities may introduce spatial
76 variations into leaf sugar $\delta^{18}\text{O}$ values that may not be fully reflected in the phloem.

77 Within the past decade, several studies have noted that phloem-exported sugars may have
78 $\delta^{18}\text{O}$ values lower than expected based on whole-leaf mean isotope ratios (Offermann et al.
79 2011; Gessler et al. 2013; Treydte et al. 2014). Where this decoupling between leaf and branch
80 isotope ratios occurs, the portion of the tree-ring signal related to leaf-level processes may be
81 attenuated, potentially influencing the interpretation of environmental variation recorded in tree-
82 ring chronologies. This study links water and soluble organic matter in needles, building on the
83 observations of significant needle water ^{18}O enrichment along the length of conifer needles
84 (Kannenberg et al. 2021). We quantified seasonal trends in the concentrations and stable isotope
85 ratios ($\delta^{18}\text{O}$ and $\delta^{13}\text{C}$) of bulk leaf organic matter, sugar, and α -cellulose along the length of
86 needles of ponderosa pine (*Pinus ponderosa*), an ecologically important and widespread western
87 US conifer that is commonly used in climate reconstructions (Leavitt et al. 2002; Watson and
88 Luckman 2002; Szejner et al. 2016; Martin et al. 2020). We hypothesize that sugar $\delta^{13}\text{C}$ values
89 will be homogenous over the leaf (reflecting similar c_i/c_a values), but that sugar $\delta^{18}\text{O}$ values will
90 express the progressive enrichment observed in leaf water $\delta^{18}\text{O}$. We also hypothesize that
91 cellulose $\delta^{13}\text{C}$ and $\delta^{18}\text{O}$ values will be homogenous across the leaf, reflecting a common
92 substrate for cellulose synthesis during needle expansion from the base.

93

94 **Materials and Methods**

95 **Study site, sample collection and preparation**

96 Samples were collected from five *P. ponderosa* individuals at the base of a southern-aspect slope
97 in Big Cottonwood Canyon, near Salt Lake City, UT (40.6°N, 111.6°W). The mean annual
98 temperature of the site is 5.7°C, and annual precipitation averages 999 mm (PRISM 1981-2010
99 climate normals, Daly et al. 2008). Temperature and precipitation at the site are highly seasonal,
100 with mean summer (JJA) temperatures of 16.5°. Moreover, only 10% of annual precipitation
101 falls during JJA, with 67% of annual precipitation falling mostly as snow between November
102 and April.

103 The most distal sections of three branches were cut from the tree at midday (between 12-2pm
104 local time) on four days during 2019: February 19, June 21, July 23, and September 14. Samples
105 were placed in a cooler containing dry ice until they could be transported back to the lab, where
106 they were kept frozen at -20°C until processed further. Needles from the prior year were
107 segmented into thirds lengthwise, microwaved at 700W for 80 seconds to inactivate enzymes and
108 oven-dried at 60°C for two days. A ~5 cm-long segment of the branch immediately adjacent to
109 the sampled needles was also microwaved and dried in the same manner as the needles. Sampled
110 branch segments were ~2 cm in diameter. After drying, the bark and phloem were separated from
111 the xylem with a razor. Needle and branch bark/phloem samples were ground in a Retsch ball
112 mill for 30 seconds at 30 Hz.

113 Leaf and xylem water isotope ratios were collected concurrently in June and September
114 (Kannenberget al. 2021). Leaf and xylem samples were placed into 20 mL vials and kept on dry
115 ice in a cooler while in the field, and then transferred to a -20°C freezer when back at the lab.

116 Xylem samples were collected from the trunk using an increment borer. Water was extracted
117 from leaf and xylem samples using cryogenic distillation until complete; leaf samples were
118 extracted for >60 minutes while stem xylem samples were extracted for >90 minutes (West et al.
119 2006). Further details of the water extraction are given in Kannenberg et al. (2021).

120

121 **Determination of sugar and starch concentrations**

122 Sugar and starch concentrations (% dry weight)—collectively referred to as non-structural
123 carbohydrates (NSC)—were determined colorimetrically (Landhäusser et al. 2018). Sugars were
124 extracted from ground samples in 80% ethanol, oxidized with a phenol-sulfuric acid solution in
125 duplicate, and solution absorbance measured at 490 nm on a Thermo Scientific Genesys20
126 visible spectrophotometer. Starch was extracted from the remaining solid sample using
127 sequential enzymatic digestion using α -amylase and amyloglucosidase. The supernatant after
128 enzymatic digestion was mixed with peroxidase-glucose oxidase (PGO) reagent in duplicate and
129 sample absorbance measured at 525 nm. More detailed protocols for these methods are found in
130 the supporting information of this article and in Landhäusser *et al.* (2018).

131

132 **Cellulose preparation and extraction**

133 Needle segments were ground to a size fraction between 35 and 60 mesh using a mortar
134 and pestle, as the ball mill technique would produce too fine a powder for subsequent extraction.
135 Branch cellulose was obtained by similarly grinding xylem from a section of branch immediately
136 adjacent to the needle samples. For each sample, ~250 mg of ground material was loaded into
137 packets made from ANKOM F57 filter bag material (ANKOM Technology; Macedon, NY).
138 Non-cellulosic components were removed from samples sequentially following established

139 methods (Leavitt and Danzer 1993; Loader et al. 1997; Rinne et al. 2005; Boettger et al. 2007).
140 Briefly, sugars and other water-soluble compounds were removed by boiling the sample in
141 deionized water for 1 hour, after which the samples were dried at 60°C overnight. Lipids, resins,
142 and other non-polar compounds were removed using Soxhlet extraction in a 2:1 toluene:ethanol
143 solution for 48 hours, and then 95% ethanol for 24 hours. After Soxhlet extraction, samples were
144 delignified using an acidified sodium chlorite solution at 70°C for 2-3 days until samples had
145 turned white. The samples were washed and boiled in deionized water to remove any remaining
146 sodium chlorite and dried at 60°C overnight. Finally, hemicelluloses were removed by soaking
147 the samples in a 17% sodium hydroxide solution for 1 hour, and then neutralized by soaking
148 samples in a 10% glacial acetic acid solution for an hour. Samples were dried in a 60°C oven
149 overnight and weighed upon removal from the sample bags to estimate the cellulose mass
150 fraction.

151

152 **Determination of isotope ratios in bulk, cellulose, and sugar fractions**

153 Samples for bulk and cellulose fractions were loaded directly into tin (for $\delta^{13}\text{C}$) and silver
154 (for $\delta^{18}\text{O}$) capsules for isotopic analysis after drying in a 60°C for 48 hours. Sugar samples were
155 isolated using a procedure similar to Brugnoli *et al.* (1988). Roughly 40 mg of bulk needle or
156 phloem material was combined with 1.75 mL of cold (2-8°C) deionized water and kept at 4°C
157 for an hour. Samples were centrifuged at 10,700 rpm for 1 min and the supernatant was passed
158 through stacked 5 mL pipette tips containing anionic and cationic exchange resins to remove
159 charged water-soluble compounds that had been co-extracted with the sugars. The upper pipette
160 tip contained DOWEX-50WX8 cation exchange resin (H^+ form, 50-100 mesh), while the lower
161 pipette tip contained DOWEX-1X8 anion exchange resin (Cl^- form, 50-100 mesh). The columns

162 were washed with 8 mL of deionized water to ensure complete elution of dissolved sugars, and
163 all eluted liquid was collected in 15 mL conical tubes. Samples were then frozen and lyophilized
164 and dissolved in 500 μ L of deionized water. Small quantities of this solution (10-30 μ L) were
165 added to pre-weighed tin (for $\delta^{13}\text{C}$) or silver (for $\delta^{18}\text{O}$) capsules. Loaded samples were then
166 frozen and lyophilized and the process repeated until at least 100 μ g (300 μ g) of material
167 remained in the silver (tin) capsules to ensure sufficient signal.

168 $\delta^{13}\text{C}$ values were determined using EA-IRMS with a Thermo Finnigan Delta Plus XL
169 coupled to a Costech EA 4010 via a Thermo Finnigan ConFlo III. A Zero Blank autosampler
170 from Costech was used to drop individual samples into the oxidation column. The helium flow
171 rate was set at 90 mL/min. Internal reference materials were two glutamic acids with different
172 carbon isotope ratios and spinach leaves, all calibrated against the USGS40 and USGS41
173 glutamic acid standards. $\delta^{18}\text{O}$ values of solid samples were determined using the glassy-carbon
174 pyrolysis method of Gehre and Strauch (2003) with a high-temperature elemental analyzer
175 (Thermo Finnigan) coupled to a ConFlo III (Thermo Finnigan) referencing interface and a
176 DeltaPlusXL isotope ratio mass spectrometer (TC/EA-IRMS, all supplied by Finnigan MAT;
177 Bremen, Germany). $\delta^{18}\text{O}$ values were calibrated to the VSMOW scale using three benzoic acid
178 standards, each having a different oxygen isotope ratio. Measurement precision of quality control
179 standards were $< 0.4\text{‰}$ (SD) for oxygen and $< 0.2\text{‰}$ (SD) for carbon.

180

181 **Statistical Analyses**

182 All data analyses were performed using R, version 4.1.1 (R Core Team 2021). Pairwise
183 differences in mean concentrations or isotope ratios were determined using repeated-measures

184 analysis of variance (ANOVA), with P values adjusted for multiple comparisons using the
185 Bonferroni correction. Data were plotted using the ggplot2 package (Wickham 2016).

186

187 **Results**

188 **Bulk isotope ratio patterns**

189 Bulk needle $\delta^{13}\text{C}$ and $\delta^{18}\text{O}$ values varied over the growing season, but differences along
190 the needle were more pronounced in $\delta^{18}\text{O}$ than in $\delta^{13}\text{C}$ (Fig. 1). Bulk $\delta^{13}\text{C}$ values were greater in
191 February than in June or July in all needle segments ($P < 0.05$, Fig 1a), except for at the needle
192 tip in July ($P = 0.102$). June and July $\delta^{13}\text{C}$ values could not be distinguished in any needle
193 segment. Gradients along the needle in $\delta^{13}\text{C}$ values were either not significant or were small. For
194 example, a $\sim 1\%$ gradient in $\delta^{13}\text{C}$ values of bulk tissue was observed in February and June. Basal
195 $\delta^{13}\text{C}$ values were higher from those in the middle and tip in February ($P < 0.001$) and were
196 higher in the needle base than the tip in June ($P < 0.002$). No pairwise differences in $\delta^{13}\text{C}$ values
197 were observed along the needle in July or September ($P > 0.11$).

198 In sharp contrast, differences across needle segments in bulk $\delta^{18}\text{O}$ values were prominent
199 (Fig. 1b). The bulk $\delta^{18}\text{O}$ values of base, middle, and tip segments were statistically distinct at all
200 four measurement periods ($P < 0.0001$, Fig. 1b), with base-to-tip differences ranging from $\sim 9\%$
201 (February) to $\sim 14\%$ (September). At the needle tip, $\delta^{18}\text{O}$ values were significantly greater along
202 each progressive measurement period by 1-2‰ ($P < 0.058$, Fig. 1b), while basal $\delta^{18}\text{O}$ values
203 varied little in June, July, and September, but were lower than in February ($P < 0.0001$).

204

205 **Seasonal changes in carbohydrate $\delta^{13}\text{C}$ and $\delta^{18}\text{O}$ values**

206 $\delta^{13}\text{C}$ values of needle cellulose were generally higher than sugar $\delta^{13}\text{C}$ values (Fig. 2ab),
207 which is consistent with prior studies (e.g., Bowling et al. 2008). Driving the bulk $\delta^{13}\text{C}$ variations
208 were changes in median sugar $\delta^{13}\text{C}$ values, which were higher in February and September than in
209 June or July (Fig. 2a). Sugar $\delta^{13}\text{C}$ values were lower in the branch phloem than in the needle (P
210 < 0.001) for all time periods. Along the needle, no significant differences were observed, with
211 the exception that February base $\delta^{13}\text{C}$ values were greater than in more distal sections of the
212 needle ($P < 0.003$). Compared to sugar $\delta^{13}\text{C}$ values, cellulose $\delta^{13}\text{C}$ values exhibited less seasonal
213 variation (Fig. 2b). Along-needle trends in cellulose $\delta^{13}\text{C}$ values were observed in February and
214 July cellulose, where $\delta^{13}\text{C}$ values were greater than in the needle midsection and tip ($P < 0.03$).
215 No along-needle cellulose $\delta^{13}\text{C}$ trends were observed in June and September ($P > 0.12$).

216 In contrast, sugar $\delta^{18}\text{O}$ values consistently exhibited progressive enrichment along the
217 needle (Fig. 2c) as all pairwise sugar $\delta^{18}\text{O}$ differences across needle segments were significant (P
218 < 0.0001 , Fig. 2c). In the basal and middle sections of the needle, sugar $\delta^{18}\text{O}$ values were largest
219 in February and September, while at the tip the highest values occurred in July (Fig. 2c). This
220 enrichment trend was strongly dampened in needle cellulose $\delta^{18}\text{O}$ values (Fig. 2d), which were
221 all within 5‰ across all sample types and times (Fig. 2d). A small gradient in $\delta^{18}\text{O}$ values of 1-
222 2‰ persisted in cellulose, with tip values being larger than middle section values in all months
223 ($P < 0.04$) and larger than basal values in June ($P < 0.0001$) and July ($P = 0.004$). Cellulose $\delta^{18}\text{O}$
224 was higher in the needle than in the branch by ~7-10‰ (Fig. 2d).

225 Relative to needle sections, sugar $\delta^{18}\text{O}$ values in the branch exhibited less variability.
226 Branch sugar $\delta^{18}\text{O}$ values were higher in June than in July ($P = 0.02$), but all other pairwise
227 comparisons across time in branch sugar $\delta^{18}\text{O}$ values were not significant. All pairwise

228 differences between needle and branch $\delta^{18}\text{O}$ values were significant ($P < 0.0007$, Fig. 2c), except
229 between the branch and needle base in June ($P = 0.06$). Progressive enrichment varied by season,
230 from a branch-needle tip difference of $\sim 15\text{‰}$ in February to nearly 25‰ in July.

231

232 **Seasonal changes in carbohydrate abundances**

233 In addition to changes in component compound isotope ratios, the observed seasonal
234 changes in bulk $\delta^{13}\text{C}$ and $\delta^{18}\text{O}$ values could have been driven by changes in carbohydrate
235 abundances within a needle. Sugar and starch abundances exhibited opposing trends during the
236 growing season, and seasonal variations in these components were larger than any potential
237 deviations along the needle. Leaf soluble sugar concentrations were higher in February ($\sim 13\%$ w
238 w^{-1}) than in June and July in all segments ($6\text{-}10\%$ w w^{-1} , $P < 0.0001$, Fig. 3a). July median sugar
239 concentrations ($\sim 10\text{-}12\%$ w w^{-1}) were greater than June median sugar concentrations ($\sim 6\text{-}8\%$ w
240 w^{-1}), but this difference was not significant ($P > 0.72$). September needle sugar concentrations
241 were lower than in February ($P < 0.01$), but larger than in June ($P < 0.004$, Fig. 3a). In the
242 branch, sugar concentrations were higher in February and September than in June and July ($P <$
243 0.03); however, February and September values were not significantly different from each other,
244 nor were June or July values ($P = 1.0$). Along the needle, no distinct variations in sugar
245 concentrations were observed ($P > 0.21$). Branch sugar concentrations were lower than in the
246 needle in February ($P < 0.001$) and July ($P < 0.01$), and in the needle middle and tip in
247 September ($P < 0.0003$).

248 Needle starch concentrations were below the detection limit in February, rose to $5\text{-}10\%$
249 (w w^{-1}) in June, and then decreased to $1\text{-}3\%$ (w w^{-1}) for July and September (Fig. 3b). June
250 needle starch concentrations were significantly higher than at all other time periods ($P < 0.001$).

251 February, July, and September needle starch concentrations were not significantly different ($P >$
252 0.06). Branch starch concentrations were also higher in June than in any other period ($P <$
253 0.001), and July starch concentrations were higher than February starch concentrations ($P <$
254 0.03). No significant differences were observed along the needle in starch concentrations ($P >$
255 0.36), though values were significantly higher than in the branch in September ($P < 0.05$).

256 The α -cellulose mass fraction was highest in February and June ($\sim 17\% \text{ w w}^{-1}$) before
257 falling to $\sim 14\text{-}15\%$ in July and $\sim 10\%$ in September (Fig. 3c). Needle cellulose percentages in
258 February and June were indistinguishable ($P = 1.0$) but were larger than in September ($P <$
259 0.003). July needle cellulose percentages were significantly lower than in February and June, and
260 significantly higher than in September at the tip ($P < 0.03$). No significant differences in
261 cellulose fraction along the needle were observed during any collection period ($P > 0.28$).

262

263 **Relationships between branch and leaf sugar $\Delta^{18}\text{O}$ and $\delta^{13}\text{C}$ values**

264 A positive but variable correlation was observed between branch and whole-leaf (e.g.,
265 averaged across the leaf) sugar $\delta^{13}\text{C}$ and $\Delta^{18}\text{O}$ values (Fig. 4ab, Table 1), but no significant
266 relationship between branch sugar $\Delta^{18}\text{O}$ and leaf water $\Delta^{18}\text{O}$ values was observed (Fig. 4c).
267 Similar relationships were observed when $\delta^{18}\text{O}$ values were used instead of $\Delta^{18}\text{O}$ values, as
268 xylem water isotope ratios only varied by $\sim 2\text{-}3\%$ throughout the observation period
269 (Kannenberget al. 2021). Over the season, $\delta^{13}\text{C}$ values in branch sugar were positively
270 correlated with those in the leaf (Fig 4a, Table 1, $r = 0.694$, $P < 0.001$). The strength of the
271 coupling between branch and leaf sugar varied throughout our measurements, with the strongest
272 coupling observed in June (Fig. 4a, Table 1, $r = 0.717$, $P = 0.02$). In contrast, the slope of the
273 relationship between branch and whole-leaf sugar $\Delta^{18}\text{O}$ values was not significant in June and

274 reached a maximum of 1.28 ± 0.39 in July ($r = 0.755$, $P = 0.012$) before decreasing to $0.91 \pm$
275 0.37 in September (Fig. 4b, Table 1, $r = 0.678$, $P = 0.004$). We did not observe any significant
276 correlation between branch sugar $\Delta^{18}\text{O}$ and leaf water $\Delta^{18}\text{O}$ values in any study period (Fig. 4c,
277 Table 1, $P > 0.07$).

278

279 **Within needle variations in sugar and leaf water $\Delta^{18}\text{O}$**

280 The relationship between midday sugar and leaf water $\Delta^{18}\text{O}$ varied across the needle (Fig.
281 5). Sugar exhibited $\Delta^{18}\text{O}$ values $\sim 30\text{‰}$ greater than leaf water $\Delta^{18}\text{O}$ values in the basal section,
282 decreasing to $\sim 18\text{-}22\text{‰}$ in the middle section (Fig. 5a). In the needle tip, sugar $\Delta^{18}\text{O}$ values were
283 $\sim 15\text{‰}$ greater than leaf water values during June, but only $\sim 7\text{‰}$ greater on average in September
284 (Fig. 5a). Segment $\Delta^{18}\text{O}$ sugar and leaf water values were highly correlated (Fig. 5b), with a
285 regression slope less than one (Table 1). The lower-than-unity slope indicates that midday leaf
286 water enrichment is damped during incorporation into photosynthetic products.

287

288 **Discussion**

289 **Phloem sugar isotope ratios may not reflect whole-needle averages in ponderosa** 290 **pine**

291 Our results are consistent with previous studies that found evidence that sugars in the
292 phloem had a lower oxygen isotope ratio than observed in leaves (Offermann et al. 2011; Gessler
293 et al. 2013; Treydte et al. 2014). These findings challenge our understanding of the extent to
294 which climatic variations recorded in the $\delta^{18}\text{O}$ values of tree-ring cellulose arise from leaf-level
295 water enrichment compared to variations in source water $\delta^{18}\text{O}$ values. Gessler et al. (2013)
296 suggested that the offset between phloem and leaf sugar values can be related to oxygen isotope

297 exchange during phloem loading and transport, as well as contributions from sugars fixed by
298 bark photosynthesis (e.g., Cernusak and Marshall 2000) which would have a $\Delta^{18}\text{O}$ value of $\sim 0\%$.
299 Our results suggest that leaf-exported assimilates most closely represent sugar $\delta^{18}\text{O}$ values near
300 the needle base in *P. ponderosa* (Fig. 2c), which raises the possibility that sugar may not be
301 equally exported from all portions of the needle, and instead might be biased toward preferential
302 export from the needle base.

303 Several factors could contribute to the apparent decoupling of phloem sugar $\Delta^{18}\text{O}$ from
304 leaf-water isotope ratios, as observed in this study. First, leaf water oxygen isotope ratios are
305 likely to be more dynamic and exhibit greater amplitude in the diel cycle than sugar oxygen
306 isotope ratios (e.g., Cernusak et al. 2005; Barnard et al. 2007; Gessler et al. 2009). As a result, it
307 would be expected that measured sugar $\Delta^{18}\text{O}$ values should reflect a dampening of midday leaf
308 water enrichment in our study, since a significant fraction of daily assimilation may have
309 occurred in the morning when $\Delta^{18}\text{O}_L$ was lower.

310 Additionally, our method of extracting sugar from the phloem may promote a further
311 dampening of the leaf-water signal. We chose to extract water soluble compounds from ground
312 phloem to maintain a consistent extraction method between leaf and phloem and also avoid
313 known issues with phloem sugar extraction (Lehmann et al. 2020). However, this method may
314 have also extracted water-soluble compounds that were not actively transported in the phloem,
315 and therefore isotope ratios may represent a mixture of assimilates of different ages and with
316 different metabolic histories. Notably, $\delta^{13}\text{C}$ and $\delta^{18}\text{O}$ of sugar alcohols tends to be lower in
317 phloem than in leaves (Rinne et al. 2015; Lehmann et al. 2017). While direct comparisons
318 between phloem and leaf sugar alcohols are sparse, it is likely that their concentration is much

319 higher in leaves (Merchant 2012), which would necessitate an even larger difference between
320 phloem and leaf sugar $\delta^{18}\text{O}$ to explain our results.

321 The temporal signal of leaf-water enrichment recorded by phloem-exported sugars may
322 also be influenced by the diel cycle of transitory starch buildup and breakdown. Chloroplast
323 starch concentrations build during the day and decrease over the night. Hydrolysis of transitory
324 starch may promote oxygen isotope exchange if intermediate products have an exposed carbonyl
325 oxygen, and at a time when $\Delta^{18}\text{O}_L$ may have much lower values than during the day (Barnard et
326 al. 2007; Gessler et al. 2008). As starch concentrations were only measured in midday samples,
327 we cannot quantify the magnitude of the starch diel cycle nor its potential to explain lower sugar
328 values observed in the branch relative to the leaf. However, offsets between branch and leaf
329 sugar $\Delta^{18}\text{O}$ values were larger when starch concentrations were lower (Fig. 2c, 3b, 5c)
330 suggesting that the starch diel cycle is unlikely to contribute significantly to this offset.

331 Gessler et al. (2013) found that sugar $\Delta^{18}\text{O}$ values in the phloem remained lower than in
332 the leaf in two pine species even after accounting for temporal variations in assimilation rates.
333 They concluded that mechanisms related to phloem loading, transport and bark photosynthesis
334 may explain the offset. There is an alternative explanation that could explain both our results and
335 those of Gessler et al. (2013). Sucrose is the dominant sugar transported by phloem and does not
336 contain carbonyl oxygen atoms capable of exchange with those in the surrounding water.
337 However, sucrose has the potential to cycle through successive transformations during transport,
338 breaking down to its monosaccharide constituents—glucose and fructose—followed by
339 reconstitution to a disaccharide. During the monosaccharide phase, up to three of the total 11
340 oxygen atoms in the sugar molecule may exchange with those in the surrounding water. Since
341 the presence of the Casparian strip within pine needles limits exchange of water between the

342 xylem and phloem in the center of the needle and the lamina (e.g., Liesche et al. 2011), the water
343 present in the central portion of the needle would likely have a lower $\Delta^{18}\text{O}$ value than in the
344 lamina (e.g., Roden et al. 2015). Thus, oxygen isotope exchange could exchange up to 3/11 of
345 the total enrichment signal recorded by sucrose synthesis in the mesophyll if two constraints are
346 met: a) sucrose is converted to glucose/fructose during or after transport across the Casparian
347 strip, and b) the water pool interior to the Casparian strip has not experienced evaporative
348 enrichment. In principle, this exchange process can only partially explain the offset between
349 phloem and needle sugar $\Delta^{18}\text{O}$ at our site. A leaf $\Delta^{18}\text{O}$ sugar value of 50‰ would correspond to a
350 phloem value of 43.7‰, assuming that 3 of 11 oxygen atoms had exchanged in isotopic
351 equilibrium with source water having $\Delta^{18}\text{O} = 0\text{‰}$.

352 The observed differences in our study, however, were considerably greater (Fig. 4b, 5c).
353 Moreover, any attenuation of the leaf-water enrichment signal is likely less than the theoretical
354 maximum, because progressive enrichment observed in leaf water $\Delta^{18}\text{O}$ requires that water
355 interior to the Casparian strip also exhibit an increase in $\Delta^{18}\text{O}$ along the needle (Farquhar and
356 Gan 2003; Shu et al. 2008; Kannenberg et al. 2021). Theoretical models for describing
357 progressive enrichment in $\Delta^{18}\text{O}_L$ suggest that the difference between basal $\Delta^{18}\text{O}_L$ and whole-leaf
358 average $\Delta^{18}\text{O}_L$ should increase with decreasing humidity (Helliker and Ehleringer 2002;
359 Farquhar and Gan 2003; Cernusak et al. 2016), implying that this effect may be particularly
360 acute in arid or semi-arid regions such as our study site.

361 Phloem transport may also contribute to the attenuation of the leaf-water $\Delta^{18}\text{O}$ signal.
362 Transport of sucrose in the phloem is ‘leaky,’ with a fraction of sucrose lost along the transport
363 pathway (van Bel 2003; De Schepper et al. 2013). Most of the leaked sucrose is reloaded into the
364 phloem, but continuous loss and reloading may result in the mixing of sucrose of different ages,

365 potentially further dampening diel climate signals transferred from leaf water to sugars (Barnard
366 et al. 2007; Gessler et al. 2009, 2014; Treydte et al. 2014). If reloading of the sucrose into the
367 phloem again involves glucose and fructose intermediates, the same three oxygen atoms in the
368 sucrose molecule can exchange again, this time in an environment with an even lower water
369 $\Delta^{18}\text{O}$. This process may also entrain sugars produced by bark photosynthesis into the phloem,
370 which would be expected to have oxygen isotope ratios 27‰ above the source water ($\Delta^{18}\text{O} =$
371 0‰) (Sternberg et al. 1986); a value much lower than that expected for leaf assimilates. Stem
372 photosynthesis has been observed in multiple conifer species (Cernusak and Marshall 2000;
373 Berveiller et al. 2007) and appears to be highest in newly grown stems. Our samples were not
374 taken from newly grown branches, but we cannot rule out contributions from stem
375 photosynthesis either from the sampled location in the branch or from newer growth further out
376 on the same branch.

377 In addition to the mechanisms raised in Gessler et al. (2013), our results raise the
378 possibility that sugars exported from the needle to the branch may be biased toward values at the
379 needle base. Some numerical models have suggested that sugar export from pine needles may be
380 basally biased (Rademaker et al. 2017). However, not all models of phloem transport in pine
381 needles arrive at this conclusion (e.g., Ronellenfitch et al. 2015). Furthermore, ^{14}C labelling
382 studies have suggested that sugar translocation speed does not vary significantly across the
383 length of individual conifer needles (Han et al. 2019), presenting a further challenge to the idea
384 of basally biased export (Rademaker et al. 2017). Therefore, it seems less likely that offsets
385 between branch and leaf sugar $\delta^{18}\text{O}$ values arise from preferential export of sugars produced at
386 the base of the needle.

387 Needle cellulose exhibited consistently greater $\delta^{18}\text{O}$ values than observed in the adjacent
388 branch, by ~7-10‰ (Fig. 2bd). Curiously, the cellulose $\delta^{18}\text{O}$ values were similar to whole-needle
389 sugar $\delta^{18}\text{O}$ values (Fig. 2cd), suggesting that spatial variations in needle $\delta^{18}\text{O}$ sugars are
390 homogenized at some point prior to incorporation into needle cellulose. Homogenization is
391 limited, however, as sugar $\delta^{18}\text{O}$ values as high as leaf cellulose were never observed in the
392 branch. Alternatively, sugars may undergo additional isotopic exchange with water in the
393 expanding needle, perhaps during cycling between hexoses and trioses (e.g., Hill et al. 1995).
394 Given that leaf water $\delta^{18}\text{O}$ values are enriched relative to water in the xylem, hexose-triose
395 cycling would increase the $\delta^{18}\text{O}$ values of sugars being incorporated into needle cellulose.
396 Models of progressive leaf water enrichment suggest that leaf water isotope ratios are more
397 sensitive to atmospheric conditions, and thus more variable, in distal portions of the needle,
398 compared to source water. As a result, water $\delta^{18}\text{O}$ values in the vicinity of leaf cellulose
399 biosynthesis near the needle base should be less sensitive to environmental variation, perhaps
400 explaining its near-constant isotope ratio along the needle, since cellulose synthesis and needle
401 expansion occur in the needle base (Kienholz 1934; Campbell 1972; Wright and Leavitt 2006).
402 This finding is consistent with recent studies in grasses that found that the $\delta^{18}\text{O}$ in cellulose and
403 $\delta^2\text{H}$ of *n*-alkanes indicated an isotope ratio of synthesis water that is lower than bulk leaf value
404 (Gamarra et al. 2016; Lehmann et al. 2017). In addition, cellulose and sugar $\delta^{18}\text{O}$ values may be
405 reflecting different time periods. For example, substrates used to construct needle cellulose may
406 have been assimilated during the previous growing season.

407

408 **Carbon isotope ratio differences from branch to needles**

409 Branch sugar $\delta^{13}\text{C}$ values were consistently $\sim 2\text{-}3\text{‰}$ lower than in the leaf (Fig. 2a). Since
410 no trend in $\delta^{13}\text{C}$ values was observed along the needle, this pattern suggests there is an apparent
411 isotopic fractionation process associated with sugars between the needle and the branch. Prior
412 studies investigating $\delta^{13}\text{C}$ values in leaves and the nearby phloem have also noted this trend
413 (Gessler et al. 2013, 2014). The observed fractionation has been attributed to post-photosynthetic
414 metabolism, such as during lignin and lipid biosynthesis (e.g., Hobbie and Werner 2004),
415 synthesis and hydrolysis of transitory starch (e.g., Brandes et al. 2006), differences in respiratory
416 fractionation, bark photosynthesis (Cernusak et al. 2009), or compartmentalization and/or mixing
417 of different carbon pools (e.g., Bögelein et al. 2019). Our results do not clarify this issue.

418 Needle cellulose exhibited consistently higher $\delta^{13}\text{C}$ values than observed in the adjacent
419 branch, by $\sim 1\text{-}3\text{‰}$ (Fig. 2bd). The $\sim 1\text{-}3\text{‰}$ offset in $\delta^{13}\text{C}$ values observed between branch and
420 needle cellulose was comparable to the difference between branch and needle sugar $\delta^{13}\text{C}$ values
421 (Fig. 2a). Since the carbon source for constructing new needle cellulose is thought to be derived
422 from carbon stored in prior years' needles (Kozlowski 1964; Dickmann and Kozlowski 1968),
423 this pattern suggests that the apparent carbon isotope fractionation associated with transport of
424 sugars from the needle to the phloem also occurs as sugars are transported into a growing needle.
425 However, a similar pattern would be expected if the expanding needle produced the sugars used
426 to construct cellulose within the same needle; our data cannot distinguish between these
427 possibilities. Moreover, the slight trend observed in cellulose $\delta^{13}\text{C}$ values along the needle
428 suggests could also arise from either or both of these processes.

429

430 **Implications for interpretations of tree-ring isotope ratios**

431 Oxygen isotope ratios of tree-ring cellulose are often interpreted to reflect both the
432 plant's source water and climatic conditions via their influence on leaf-level processes (e.g.,
433 McCarroll and Loader 2004; Reynolds-Henne et al. 2007; Treydte et al. 2007; Saurer et al. 2012;
434 Vitali et al. 2021). Our data, consistent with several other studies (Treydte et al. 2014; Gessler et
435 al. 2014; Cheesman and Cernusak 2016; Miranda et al. 2021), suggest the ways through which
436 the leaf-water signal is ultimately recorded in wood cellulose may be more complicated than
437 expressed in current models. While Treydte et al. (2014) found reliable relationships between
438 climate variations and tree-ring cellulose $\delta^{18}\text{O}$, they noted that such relations should be strongest
439 in humid regions with precipitation maxima during the growing season. Miranda et al. (2021)
440 reported general consistency with model predictions in trends between climate variation and tree-
441 ring cellulose $\delta^{18}\text{O}$ and $\delta^{13}\text{C}$ along a sharp altitudinal gradient in the Canary Islands, even at the
442 least humid sites. Other studies, however, have shown that while general trends in cellulose
443 isotope values follow large environmental gradients, the process-based modeling of isotope
444 values through the component chains from leaf water pools through sucrose to cellulose are not
445 easily resolved (Schmidt et al. 2001; Lehmann et al. 2017). Modeling is likely to be confounded
446 by species- and tissue-specific dynamics and post-assimilation processes, as well as unique
447 dependencies on the atmospheric environment. Our results highlight the importance of resolving
448 how within-needle fractionation gradients transfer from leaf water pools to the tree-ring record.

449 Progressive leaf-water enrichment models suggest that the leaf water environment varies
450 weakly with atmospheric conditions at the base of the leaf and that leaf water $\delta^{18}\text{O}$ values are far
451 more sensitive to atmospheric changes at the leaf tip (Farquhar and Gan 2003; Shu et al. 2008;
452 Kannenberg et al. 2021). We suspect that the decoupling between whole-leaf and phloem sugar
453 $\delta^{18}\text{O}$ is most significant in arid conditions, as these conditions promote the largest-magnitude of

454 base-to-tip water $\delta^{18}\text{O}$ heterogeneities (Helliker and Ehleringer 2002; Farquhar and Gan 2003;
455 Shu et al. 2008; Kannenberg et al. 2021). An additional damping of the leaf water signal was
456 reported in the Barbour and Farquhar (2000) model relating leaf-water isotope ratios to tree-ring
457 cellulose and can be accounted for by allowing the p_{ex} parameter to vary. However, our results
458 and the results of prior studies (Offermann et al. 2011; Gessler et al. 2013; Treydte et al. 2014)
459 caution that these apparent variations in p_{ex} may not solely reflect variations in the degree of
460 hexose-triose cycling, and that multiple physiological processes may instead be responsible.

461

462 **Conclusions**

463 Models of tree-ring cellulose isotope ratios often rely on predictions of whole-leaf water
464 isotope ratios. However, spatial heterogeneity in leaf water isotope ratios is common and could
465 bias these relationships if exported sugars do not reflect whole-leaf values. In our study of
466 ponderosa pine, we found that branch $\delta^{13}\text{C}$ and $\delta^{18}\text{O}$ values in exported sugars were distinct from
467 whole-needle values. Offsets in sugar $\delta^{13}\text{C}$ values were fixed and did not vary with position in
468 the leaf, but a small along-needle trend was observed in cellulose. This effect most likely reflects
469 mixing of multiple carbon pools or effects of post-photosynthetic metabolism (Hobbie and
470 Werner 2004; Brandes et al. 2006; Bögelein et al. 2019), and perhaps variations in environmental
471 conditions during needle expansion (Wright and Leavitt, 2006). In contrast, needle sugar $\delta^{18}\text{O}$
472 values expressed a progressive enrichment in $\delta^{18}\text{O}$ from base to tip. We conclude that the origin
473 of this gradient in needle sugar $\delta^{18}\text{O}$ arises from the progressive increase in leaf water $\delta^{18}\text{O}$
474 during initial sugar synthesis. The $\delta^{18}\text{O}$ of sugars exported from the leaf do not appear to reflect
475 whole-leaf averages and instead are most similar to sugars at the needle base, in contrast to
476 commonly applied cellulose isotope models. This offset between branch and needle likely arises

477 from oxygen isotope exchange during phloem loading and transport, and may be further
478 augmented in the branch by contributions from stem photosynthesis. The presence of oxygen
479 isotope ratio gradients in leaf sugars, and the apparent lack of these gradients in conifer needle
480 cellulose, presents a new opportunity for tracing isotope ratio signals from sugars to their
481 incorporation in sink tissues and improving cellulose isotope ratio models.

482

483 **Acknowledgments**

484 We thank Avery W. Driscoll and Nic Bitter for field assistance, and Hayley G. Lind, Sierra
485 Hymas, and Suvankar Chakraborty for laboratory assistance.

486

487 **Declarations:**

488 **Funding:** RPF, SAK, WRLA, and JRE were supported by the National Science Foundation
489 (NSF) under grant number 1753845; RKM was supported by NSF grant number 1754430. RPF
490 and WRLA also received support from NSF grant number 1802880. RPF also acknowledges
491 support from NSF grant number 1954660 and WRLA acknowledges support from the David and
492 Lucille Packard Foundation, NSF grant number 1714972, and the United States Department of
493 Agriculture under grant number 2018-67019-27850.

494 **Conflicts of interest:** The authors declare that they have no conflicts of interest.

495 **Data availability statement:** The isotope ratio and chemical abundance data that support the
496 findings of this study are openly available in figshare at
497 <http://doi.org/10.6084/m9.figshare.13394870>. Climatological data are available from the PRISM
498 (Parameter-elevation Regressions on Independent Slopes Model) Climate Group as part of the
499 Norm81m data product at prism.oregonstate.edu.

500 **References**

- 501 Babst F, Alexander MR, Szejner P, Bouriaud O, Klesse S, Roden J, et al. (2014) A tree-ring
502 perspective on the terrestrial carbon cycle. *Oecologia* 176:307–322.
503 <https://doi.org/10.1007/s00442-014-3031-6>
- 504 Barbour MM (2007) Stable oxygen isotope composition of plant tissue: a review. *Funct Plant*
505 *Biol* 34:83. <https://doi.org/10.1071/FP06228>
- 506 Barbour MM, Farquhar GD (2000) Relative humidity- and ABA- induced variation in carbon
507 and oxygen isotope ratios of cotton leaves. *Plant Cell Environ* 23:473–485.
508 <https://doi.org/10.1046/j.1365-3040.2000.00575.x>
- 509 Barnard RL, Salmon Y, Kodama N, Sörgel K, Holst J, Rennenberg H, et al. (2007) Evaporative
510 enrichment and time lags between $\delta^{18}\text{O}$ of leaf water and organic pools in a pine stand.
511 *Plant Cell Environ* 30:539–550. <https://doi.org/10.1111/j.1365-3040.2007.01654.x>
- 512 Benner R, Fogel ML, Sprague EK, Hodson RE (1987) Depletion of ^{13}C in lignin and its
513 implications for stable carbon isotope studies. *Nature* 329:708–710.
514 <https://doi.org/10.1038/329708a0>
- 515 Berveiller D, Kierzkowski D, Damesin C (2007) Interspecific variability of stem photosynthesis
516 among tree species. *Tree Physiol* 27:53–61. <https://doi.org/10.1093/treephys/27.1.53>
- 517 Boettger T, Haupt M, Knöller K, Weise SM, Waterhouse JS, Rinne KT, et al. (2007) Wood
518 Cellulose Preparation Methods and Mass Spectrometric Analyses of $\delta^{13}\text{C}$, $\delta^{18}\text{O}$, and
519 Nonexchangeable $\delta^2\text{H}$ Values in Cellulose, Sugar, and Starch: An Interlaboratory
520 Comparison. *Anal Chem* 79:4603–4612. <https://doi.org/10.1021/ac0700023>

521 Bögelein R, Lehmann MM, Thomas FM (2019) Differences in carbon isotope leaf-to-phloem
522 fractionation and mixing patterns along a vertical gradient in mature European beech and
523 Douglas fir. *New Phytol.* <https://doi.org/10.1111/nph.15735>

524 Bowling DR, Pataki DE, Randerson JT (2008) Carbon isotopes in terrestrial ecosystem pools and
525 CO₂ fluxes. *New Phytol* 178:24–40. <https://doi.org/10.1111/j.1469-8137.2007.02342.x>

526 Brandes E, Kodama N, Whittaker K, Weston C, Rennenberg H, Keitel C, et al. (2006) Short-
527 term variation in the isotopic composition of organic matter allocated from the leaves to
528 the stem of *Pinus sylvestris*: effects of photosynthetic and postphotosynthetic carbon
529 isotope fractionation. *Glob Change Biol* 12:1922–1939. [https://doi.org/10.1111/j.1365-](https://doi.org/10.1111/j.1365-2486.2006.01205.x)
530 [2486.2006.01205.x](https://doi.org/10.1111/j.1365-2486.2006.01205.x)

531 Brugnoli E, Hubick KT, von Caemmerer S, Wong SC, Farquhar GD (1988) Correlation between
532 the Carbon Isotope Discrimination in Leaf Starch and Sugars of C₃ Plants and the Ratio
533 of Intercellular and Atmospheric Partial Pressures of Carbon Dioxide. *Plant Physiol*
534 88:1418–1424. <https://doi.org/10.1104/pp.88.4.1418>

535 Campbell R (1972) Electron Microscopy of the Development of Needles of *Pinus nigra* var.
536 *maritima*. *Ann Bot* 36:711–720. <https://doi.org/10.1093/oxfordjournals.aob.a084627>

537 Cernusak LA, Barbour MM, Arndt SK, Cheesman AW, English NB, Field TS, et al. (2016)
538 Stable isotopes in leaf water of terrestrial plants. *Plant Cell Environ* 39:1087–1102.
539 <https://doi.org/10.1111/pce.12703>

540 Cernusak LA, Farquhar GD, Pate JS (2005) Environmental and physiological controls over
541 oxygen and carbon isotope composition of Tasmanian blue gum, *Eucalyptus globulus*.
542 *Tree Physiol* 25:129–146. <https://doi.org/10.1093/treephys/25.2.129>

543 Cernusak LA, Marshall JD (2000) Photosynthetic refixation in branches of Western White Pine.
544 *Funct Ecol* 14:300–311. <https://doi.org/10.1046/j.1365-2435.2000.00436.x>

545 Cernusak LA, Marshall JD, Comstock JP, Balster NJ (2001) Carbon isotope discrimination in
546 photosynthetic bark. *Oecologia* 128:24–35. <https://doi.org/10.1007/s004420100629>

547 Cernusak LA, Tcherkez G, Keitel C, Cornwell WK, Santiago LS, Knohl A, et al. (2009) Why are
548 non-photosynthetic tissues generally ^{13}C enriched compared with leaves in C_3 plants?
549 Review and synthesis of current hypotheses. *Funct Plant Biol* 36:199.
550 <https://doi.org/10.1071/FP08216>

551 Cernusak LA, Wong SC, Farquhar GD (2003) Oxygen isotope composition of phloem sap in
552 relation to leaf water in *Ricinus communis*. *Funct Plant Biol* 30:1059.
553 <https://doi.org/10.1071/FP03137>

554 Cheesman AW, Cernusak LA (2016) Infidelity in the outback: climate signal recorded in $\Delta^{18}\text{O}$ of
555 leaf but not branch cellulose of eucalypts across an Australian aridity gradient. *Tree*
556 *Physiol.* <https://doi.org/10.1093/treephys/tpw121>

557 Cook ER, Anchukaitis KJ, Buckley BM, D'Arrigo RD, Jacoby GC, Wright WE (2010) Asian
558 Monsoon Failure and Megadrought During the Last Millennium. *Science* 328:486–489.
559 <https://doi.org/10.1126/science.1185188>

560 Daly C, Halbleib M, Smith JI, Gibson WP, Doggett MK, Taylor GH, et al. (2008)
561 Physiographically sensitive mapping of climatological temperature and precipitation
562 across the conterminous United States. *Int J Climatol* 28:2031–2064

563 Danis PA, Masson-Delmotte V, Stievenard M, Guillemin MT, Daux V, Naveau P, et al. (2006)
564 Reconstruction of past precipitation $\delta^{18}\text{O}$ using tree-ring cellulose $\delta^{18}\text{O}$ and $\delta^{13}\text{C}$: A

565 calibration study near Lac d'Annecy, France. *Earth Planet Sci Lett* 243:439–448.
566 <https://doi.org/10.1016/j.epsl.2006.01.023>

567 D'Arrigo R, Villalba R, Wiles G (2001) Tree-ring estimates of Pacific decadal climate
568 variability. *Clim Dyn* 18:219–224

569 De Schepper V, De Swaef T, Bauweraerts I, Steppe K (2013) Phloem transport: a review of
570 mechanisms and controls. *J Exp Bot* 64:4839–4850. <https://doi.org/10.1093/jxb/ert302>

571 Dickmann DI, Kozlowski TT (1968) Mobilization by *Pinus resinosa* Cones and Shoots of C14-
572 Photosynthate from Needles of Different Ages. *Am J Bot* 55:900–906

573 English NB, Dettman DL, Sandquist DR, Williams DG (2007) Past climate changes and
574 ecophysiological responses recorded in the isotope ratios of saguaro cactus spines.
575 *Oecologia* 154:247–258. <https://doi.org/10.1007/s00442-007-0832-x>

576 Farquhar GD, Ehleringer JR, Hubick KT (1989) Carbon Isotope Discrimination and
577 Photosynthesis. *Annu Rev Plant Physiol Plant Mol Biol* 40:503–537

578 Farquhar GD, Gan KS (2003) On the progressive enrichment of the oxygen isotopic composition
579 of water along a leaf: Leaf water isotope modelling. *Plant Cell Environ* 26:1579–1597.
580 <https://doi.org/10.1046/j.0016-8025.2001.00829.x-i1>

581 Frank DC, Poulter B, Saurer M, Esper J, Huntingford C, Helle G, Treydte K, et al. (2015) Water-
582 use efficiency and transpiration across European forests during the Anthropocene. *Nat*
583 *Clim Change* 5:579–583. <https://doi.org/10.1038/nclimate2614>

584 Gamarra B, Sachse D, Kahmen A (2016) Effects of leaf water evaporative ²H-enrichment and
585 biosynthetic fractionation on leaf wax *n*-alkane $\delta^2\text{H}$ values in C3 and C4 grasses. *Plant*
586 *Cell Environ* 39:2390–2403. <https://doi.org/10.1111/pce.12789>

587 Gehre M, Strauch G (2003) High-temperature elemental analysis and pyrolysis techniques for
588 stable isotope analysis. *Rapid Commun Mass Spectrom* 17:1497–1503.
589 <https://doi.org/10.1002/rcm.1076>

590 Gessler A, Brandes E, Buchmann N, Helle G, Rennenberg H, Barnard RL (2009) Tracing carbon
591 and oxygen isotope signals from newly assimilated sugars in the leaves to the tree-ring
592 archive. *Plant Cell Environ* 32:780–795. [https://doi.org/10.1111/j.1365-
593 3040.2009.01957.x](https://doi.org/10.1111/j.1365-3040.2009.01957.x)

594 Gessler A, Brandes E, Keitel C, Boda S, Kayler ZE, Granier A, et al. (2013) The oxygen isotope
595 enrichment of leaf-exported assimilates - does it always reflect lamina leaf water
596 enrichment? *New Phytol* 200:144–157. <https://doi.org/10.1111/nph.12359>

597 Gessler A, Ferrio JP, Hommel R, Treydte K, Werner RA, Monson RK (2014) Stable isotopes in
598 tree rings: towards a mechanistic understanding of isotope fractionation and mixing
599 processes from the leaves to the wood. *Tree Physiol* 34:796–818.
600 <https://doi.org/10.1093/treephys/tpu040>

601 Gessler A, Tcherkez G, Peuke AD, Ghashghaie J, Farquhar GD (2008) Experimental evidence
602 for diel variations of the carbon isotope composition in leaf, stem and phloem sap organic
603 matter in *Ricinus communis*. *Plant Cell Environ* 31:941–953.
604 <https://doi.org/10.1111/j.1365-3040.2008.01806.x>

605 Han X, Turgeon R, Schulz A, Liesche J (2019) Environmental conditions, not sugar export
606 efficiency, limit the length of conifer leaves. *Tree Physiol* 39:312–319.
607 <https://doi.org/10.1093/treephys/tpy056>

608 Helliker BR, Ehleringer JR (2000) Establishing a grassland signature in veins: ^{18}O in the leaf
609 water of C3 and C4 grasses. *Proc Natl Acad Sci* 97:7894–7898.
610 <https://doi.org/10.1073/pnas.97.14.7894>

611 Helliker BR, Ehleringer JR (2002) Differential ^{18}O enrichment of leaf cellulose in C3 versus C4
612 grasses. *Funct Plant Biol* 29:435. <https://doi.org/10.1071/PP01122>

613 Hill SA, Waterhouse JS, Field EM, Switsur VR, Ap Rees T (1995) Rapid recycling of triose
614 phosphates in oak stem tissue. *Plant Cell Environ* 18:931–936.
615 <https://doi.org/10.1111/j.1365-3040.1995.tb00603.x>

616 Hobbie EA, Werner RA (2004) Intramolecular, compound-specific, and bulk carbon isotope
617 patterns in C₃ and C₄ plants: a review and synthesis. *New Phytol* 161:371–385.
618 <https://doi.org/10.1111/j.1469-8137.2004.00970.x>

619 Kahmen A, Sachse D, Arndt SK, Tu KP, Farrington H, Vitousek PM, et al. (2011) Cellulose
620 $\delta^{18}\text{O}$ is an index of leaf-to-air vapor pressure difference (VPD) in tropical plants. *Proc*
621 *Natl Acad Sci* 108:1981–1986. <https://doi.org/10.1073/pnas.1018906108>

622 Kannenberg SA, Fiorella RP, Anderegg WRL, Monson RK, Ehleringer JR (2021) Seasonal and
623 diurnal trends in progressive isotope enrichment along needles in two pine species. *Plant*
624 *Cell Environ* 44:143–155. <https://doi.org/10.1111/pce.13915>

625 Kienholz R (1934) Leader, Needle, Cambial, and Root Growth of Certain Conifers and Their
626 Interrelations. *Bot Gaz* 96:73–92. <https://doi.org/10.1086/334447>

627 Kozlowski TT (1964) Shoot growth in woody plants. *Bot Rev* 30:335–392.
628 <https://doi.org/10.1007/BF02858538>

629 Landhäusser SM, Chow PS, Dickman LT, Furze ME, Kuhlman I, Schmid S, et al. (2018)
630 Standardized protocols and procedures can precisely and accurately quantify non-

631 structural carbohydrates. *Tree Physiol* 38:1764–1778.
632 <https://doi.org/10.1093/treephys/tpy118>

633 Leavitt SW, Danzer SR (1993) Method for batch processing small wood samples to
634 holocellulose for stable-carbon isotope analysis. *Anal Chem* 65:87–89.
635 <https://doi.org/10.1021/ac00049a017>

636 Leavitt SW, Wright WE, Long A (2002) Spatial expression of ENSO, drought, and summer
637 monsoon in seasonal $\delta^{13}\text{C}$ of ponderosa pine tree rings in southern Arizona and New
638 Mexico. *J Geophys Res* 107:4349. <https://doi.org/10.1029/2001JD001312>

639 Lehmann MM, Gamarra B, Kahmen A, Siegwolf RTW, Saurer M (2017) Oxygen isotope
640 fractionations across individual leaf carbohydrates in grass and tree species: $\delta^{18}\text{O}$ of
641 individual leaf carbohydrates. *Plant Cell Environ* 40:1658–1670.
642 <https://doi.org/10.1111/pce.12974>

643 Lehmann MM, Goldsmith GR, Miranda- Ney C, Weigt RB, Schönbeck L, Kahmen A, et al.
644 (2020) The ^{18}O - signal transfer from water vapour to leaf water and assimilates varies
645 among plant species and growth forms. *Plant Cell Environ* 43:510–523.
646 <https://doi.org/10.1111/pce.13682>

647 Libby LM, Pandolfi LJ, Payton PH, Marshall J, Becker B, Giertz-Sienbenlist V (1976) Isotopic
648 tree thermometers. *Nature* 261:284–288. <https://doi.org/10.1038/261284a0>

649 Liesche J, Martens HJ, Schulz A (2011) Symplasmic transport and phloem loading in
650 gymnosperm leaves. *Protoplasma* 248:181–190. [https://doi.org/10.1007/s00709-010-](https://doi.org/10.1007/s00709-010-0239-0)
651 0239-0

652 Loader NJ, Robertson I, Barker AC, Switsur VR, Waterhouse JS (1997) An improved technique
653 for the batch processing of small wholewood samples to alpha cellulose. *Chem Geol*
654 136:313–317

655 Martin JT, Pederson GT, Woodhouse CA, Cook ER, McCabe G, Anchukaitis KJ, et al. (2020)
656 Increased drought severity tracks warming in the United States' largest river basin. *Proc*
657 *Natl Acad Sci* 117:11328–11336. <https://doi.org/10.1073/pnas.1916208117>

658 Mathias JM, Thomas RB (2021) Global tree intrinsic water use efficiency is enhanced by
659 increased atmospheric CO₂ and modulated by climate and plant functional types. *Proc*
660 *Natl Acad Sci* 118:e2014286118. <https://doi.org/10.1073/pnas.2014286118>

661 McCarroll D, Loader NJ (2004) Stable isotopes in tree rings. *Quat Sci Rev* 23:771–801.
662 <https://doi.org/10.1016/j.quascirev.2003.06.017>

663 Merchant A (2012) Developing Phloem δ¹³C and Sugar Composition as Indicators of Water
664 Deficit in *Lupinus angustifolius*. *HortScience* 47:6.
665 <https://doi.org/10.21273/HORTSCI.47.6.691>

666 Miranda JC, Lehmann MM, Saurer M, Altman J, Treydte K (2021) Insight into Canary Island
667 pine physiology provided by stable isotope patterns of water and plant tissues along an
668 altitudinal gradient. *Tree Physiol* 00:1–16. <https://doi.org/10.1093/treephys/tpab046>

669 Offermann C, Ferrio JP, Holst J, Grote R, Siegwolf R, Kayler Z, et al. (2011) The long way
670 down--are carbon and oxygen isotope signals in the tree ring uncoupled from canopy
671 physiological processes? *Tree Physiol* 31:1088–1102.
672 <https://doi.org/10.1093/treephys/tpr093>

673 R Core Team (2021) R: A Language and Environment for Statistical Computing. R Foundation
674 for Statistical Computing, Vienna, Austria

675 Rademaker H, Zwieniecki MA, Bohr T, Jensen KH (2017) Sugar export limits size of conifer
676 needles. *Phys Rev E* 95:042402. <https://doi.org/10.1103/PhysRevE.95.042402>

677 Reynolds-Henne CE, Siegwolf RTW, Treydte KS, Esper J, Henne S, Saurer M (2007) Temporal
678 stability of climate-isotope relationships in tree rings of oak and pine (Ticino,
679 Switzerland). *Glob Biogeochem Cycles* 21:GB4009.
680 <https://doi.org/10.1029/2007GB002945>

681 Rinne KT, Boettger T, Loader NJ, Robertson I, Switsur, VR, Waterhouse JS (2005) On the
682 purification of α -cellulose from resinous wood for stable isotope (H, C and O) analysis.
683 *Chem Geol* 222:75–82. <https://doi.org/10.1016/j.chemgeo.2005.06.010>

684 Rinne KT, Saurer M, Kirilyanov AV, Bruyukhanova MV, Prokushkin AS, Churakova
685 (Sidorova), OV et al. (2015) Examining the response of needle carbohydrates from
686 Siberian larch trees to climate using compound-specific $\delta^{13}\text{C}$ and concentration analyses.
687 *Plant Cell Environ* 38:2340–2352. <https://doi.org/10.1111/pce.12554>

688 Roden J, Kahmen A, Buchmann N, Siegwolf R (2015) The enigma of effective path length for
689 ^{18}O enrichment in leaf water of conifers. *Plant Cell Environ* 38:2551–2565.
690 <https://doi.org/10.1111/pce.12568>

691 Roden JS, Ehleringer JR (2007) Summer precipitation influences the stable oxygen and carbon
692 isotopic composition of tree-ring cellulose in *Pinus ponderosa*. *Tree Physiol* 27:491–501.
693 <https://doi.org/10.1093/treephys/27.4.491>

694 Roden JS, Lin G, Ehleringer JR (2000) A mechanistic model for interpretation of hydrogen and
695 oxygen isotope ratios in tree-ring cellulose. *Geochim Cosmochim Acta* 64:21–35.
696 [https://doi.org/10.1016/S0016-7037\(99\)00195-7](https://doi.org/10.1016/S0016-7037(99)00195-7)

697 Ronellenfitch H, Liesche J, Jensen KH, Holbrook NM, Schulz A, Katifori E (2015) Scaling of
698 phloem structure and optimality of photoassimilate transport in conifer needles. *Proc R*
699 *Soc B Biol Sci* 282:20141863. <https://doi.org/10.1098/rspb.2014.1863>

700 Šantrůček J, Květoň J, Šetlík J, Bulíčková L (2007) Spatial Variation of Deuterium Enrichment
701 in Bulk Water of Snowgum Leaves. *Plant Physiol* 143:88–97.
702 <https://doi.org/10.1104/pp.106.089284>

703 Saurer M, Aellen K, Siegwolf R (1997) Correlating $\delta^{13}\text{C}$ and $\delta^{18}\text{O}$ in cellulose of trees. *Plant*
704 *Cell Environ* 20:1543–1550

705 Saurer M, Kress A, Leuenberger M, Rinne KT, Treydte KS, Siegwolf RTW (2012) Influence of
706 atmospheric circulation patterns on the oxygen isotope ratio of tree rings in the Alpine
707 region. *J Geophys Res Atmospheres* 117, D05118.
708 <https://doi.org/10.1029/2011JD016861>

709 Saurer M, Spahni R, Frank DC, Joos F, Leuenberger M, Loader NJ, et al. (2014) Spatial
710 variability and temporal trends in water-use efficiency of European forests. *Glob Change*
711 *Biol* 20:3700–3712. <https://doi.org/10.1111/gcb.12717>

712 Schmidt H-L, Werner RA, Roßmann A (2001) ^{18}O Pattern and biosynthesis of natural plant
713 products. *Phytochemistry* 58:9–32. [https://doi.org/10.1016/S0031-9422\(01\)00017-6](https://doi.org/10.1016/S0031-9422(01)00017-6)

714 Shu Y, Feng X, Posmentier ES, Sonder LJ, Faiia AM, Yakir D (2008) Isotopic studies of leaf
715 water. Part 1: A physically based two-dimensional model for pine needles. *Geochim*
716 *Cosmochim Acta* 72:5175–5188. <https://doi.org/10.1016/j.gca.2008.05.062>

717 Sidorova OV, Siegwolf RTW, Saurer M, Shashkin AV, Knorre AA, Prokushkin AS, et al. (2009)
718 Do centennial tree-ring and stable isotope trends of *Larix gmelinii* (Rupr.) Rupr. indicate

719 increasing water shortage in the Siberian north? *Oecologia* 161:825–835.
720 <https://doi.org/10.1007/s00442-009-1411-0>

721 Sternberg LDSL, Deniro MJ, Savidge RA (1986) Oxygen Isotope Exchange between
722 Metabolites and Water during Biochemical Reactions Leading to Cellulose Synthesis.
723 *Plant Physiol* 82:423–427. <https://doi.org/10.1104/pp.82.2.423>

724 Szejner P, Wright WE, Babst F, Belmecheri S, Trouet V, Leavitt SW, et al. (2016) Latitudinal
725 gradients in tree ring stable carbon and oxygen isotopes reveal differential climate
726 influences of the North American Monsoon System: Intra-annual Tree Ring C and O
727 Isotopes. *J Geophys Res Biogeosciences* 121:1978–1991.
728 <https://doi.org/10.1002/2016JG003460>

729 Treydte K, Boda S, Graf Pannatier E, Fonti P, Frank D, Ullrich B, et al. (2014) Seasonal transfer
730 of oxygen isotopes from precipitation and soil to the tree ring: source water versus needle
731 water enrichment. *New Phytol* 202:772–783. <https://doi.org/10.1111/nph.12741>

732 Treydte K, Frank D, Esper J, Andreu L, Bednarz Z, Berninger F, et al. (2007) Signal strength and
733 climate calibration of a European tree-ring isotope network. *Geophys Res Lett*
734 34:L24302. <https://doi.org/10.1029/2007GL031106>

735 Treydte KS, Schleser GH, Helle G, Frank DC, Winiger M, Haug GH, et al. (2006) The twentieth
736 century was the wettest period in northern Pakistan over the past millennium. *Nature*
737 440:1179–1182. <https://doi.org/10.1038/nature04743>

738 van Bel AJE (2003) The phloem, a miracle of ingenuity. *Plant Cell Environ* 26:125–149

739 Vitali V, Klesse S, Weigt R, Treydte K, Frank D, Saurer M, et al. (2021) High-frequency stable
740 isotope signals in uneven-aged forests as proxy for physiological responses to climate in
741 Central Europe. *Tree Physiol* 00, 1-17. <https://doi.org/10.1093/treephys/tpab062>

742 Watson E, Luckman BH (2002) The dendroclimatic signal in Douglas-fir and ponderosa pine
743 tree-ring chronologies from the southern Canadian Cordillera. *Can J For Res* 32:1858–
744 1874

745 West AG, Patrickson SJ, Ehleringer JR (2006) Water extraction times for plant and soil materials
746 used in stable isotope analysis. *Rapid Commun Mass Spectrom* 20:1317–1321.
747 <https://doi.org/10.1002/rcm.2456>

748 Wickham H (2016) *ggplot2: Elegant graphics for data analysis*. Springer-Verlag New York

749 Williams AP, Cook ER, Smerdon JE, Cook BI, Abatzoglou JT, Bolles K, et al. (2020) Large
750 contribution from anthropogenic warming to an emerging North American megadrought.
751 *Science* 368:314–318. <https://doi.org/10.1126/science.aaz9600>

752 Wright WE, Leavitt SW (2006) Needle cell elongation and maturation timing derived from pine
753 needle cellulose $\delta^{18}\text{O}$. *Plant Cell Environ* 29:1–14. [https://doi.org/10.1111/j.1365-
754 3040.2005.01394.x](https://doi.org/10.1111/j.1365-3040.2005.01394.x)

755

756 **Tables**

757 Table 1. Seasonal variations in carbon and water isotope ratios between branch and leaf across

758 leaf water and sugars. Regressions significant at the $P = 0.05$ level are printed in bold.

$\delta^{13}\text{C}$, branch and whole-leaf sugar	Slope	Intercept	P value	Correlation
February	0.49 ± 0.25	-14.87 ± 6.00	0.068	0.483
June	0.89 ± 0.31	-4.33 ± 8.20	0.020	0.717
July	0.31 ± 0.16	-19.59 ± 4.09	0.086	0.569
September	0.32 ± 0.46	-19.26 ± 11.51	0.51	0.253
Pooled – all data	0.53 ± 0.08	-14.01 ± 2.12	< 0.001	0.697
$\Delta^{18}\text{O}$, branch sugar and leaf water	Slope	Intercept	P value	Correlation
June	0.52 ± 0.26	26.04 ± 6.59	0.078	0.582
September	-0.09 ± 0.56	38.59 ± 15.53	0.88	-0.057
Pooled – all data	-0.12 ± 0.21	41.12 ± 5.74	0.55	-0.113
$\Delta^{18}\text{O}$, branch and whole-leaf sugar	Slope	Intercept	P value	Correlation
June	0.15 ± 0.46	31.75 ± 22.90	0.75	0.117
July	1.28 ± 0.39	-27.01 ± 19.85	0.012	0.755
September	0.91 ± 0.37	-9.40 ± 18.48	0.004	0.678
Pooled – all data	0.95 ± 0.30	-10.00 ± 15.12	0.004	0.519
$\Delta^{18}\text{O}$, sugar and water in segments	Slope	Intercept	P value	Correlation

June	0.57 ± 0.01	34.10 ± 0.44	< 0.001	0.991
September	0.40 ± 0.02	37.26 ± 0.65	< 0.001	0.973
Pooled – all data	0.46 ± 0.02	36.34 ± 0.57	< 0.001	0.962

760 **Figure Legends**

761 **Fig. 1** Boxplots of a) $\delta^{13}\text{C}$ and b) $\delta^{18}\text{O}$ values of bulk organic matter across all needle segments
762 and sampling dates. The horizontal line in each boxplot corresponds to the median isotope ratio,
763 the boxes span the 25th-75th percentiles. Whiskers represent values within 1.5-times of the inter-
764 quartile range (IQR) of the median, and outliers are shown as circles. Boxplot fill colors indicate
765 sampling dates.

766

767 **Fig. 2** Boxplots of sugar a) $\delta^{13}\text{C}$ and b) $\delta^{18}\text{O}$ values of in needle segments (base, middle, or tip)
768 and proximal branch phloem, and c) $\delta^{13}\text{C}$ and d) $\delta^{18}\text{O}$ values in needle segment and proximal
769 branch cellulose. The horizontal line in each boxplot corresponds to the median isotope ratio, the
770 boxes span the 25th-75th percentiles. Whiskers represent values within 1.5-times of the IQR of the
771 median, and outliers are shown as circles. Boxplot fill colors indicate sampling dates.

772

773 **Fig. 3** Percentage of branch and needle segment (base, middle, or tip) dry mass corresponding to
774 a) soluble sugars, b) starch, and c) α -cellulose. The horizontal line in each boxplot corresponds
775 to the median isotope ratio, the boxes span the 25th-75th percentiles. Whiskers represent values
776 within 1.5-times of the IQR of the median, and outliers are shown as circles. Boxplot fill colors
777 indicate sampling dates.

778

779 **Fig. 4** Relationships between: a) branch and needle sugar $\delta^{13}\text{C}$, and branch sugar $\Delta^{18}\text{O}$ with b)
780 whole-leaf sugar $\Delta^{18}\text{O}$ and c) whole-leaf water $\Delta^{18}\text{O}_L$. Best-fit lines are shown when the
781 regressions are significant ($P < 0.05$). February values for $\Delta^{18}\text{O}_L$ and $\Delta^{18}\text{O}_{\text{sugar}}$ were not
782 calculated and are missing from panels b) and c), as no xylem or leaf water samples were

783 collected during this time. Colors and symbols indicate sampling period (February – light blue
784 circles, June – dark blue triangle, July – light green squares, September – dark green crosses).

785

786 **Fig. 5** Relationships between $\Delta^{18}\text{O}$ of needle water and sugar: a) differences between $\Delta^{18}\text{O}_{\text{sugar}}$
787 and $\Delta^{18}\text{O}_{\text{L}}$ by segment, b) relationship between $\Delta^{18}\text{O}_{\text{sugar}}$ and concurrent $\Delta^{18}\text{O}_{\text{L}}$ in the same
788 needle segment, and c) branch and needle $\Delta^{18}\text{O}_{\text{sugar}}$ in the whole needle (circle) and the basal
789 third only (triangles). The solid black line in panel c) represents the expected equilibrium ^{18}O -
790 enrichment of sugars above leaf water, $\Delta^{18}\text{O}_{\text{sugar}} = 1.027\Delta^{18}\text{O}_{\text{L}} + 27\text{‰}$ (e.g., Barbour 2007).

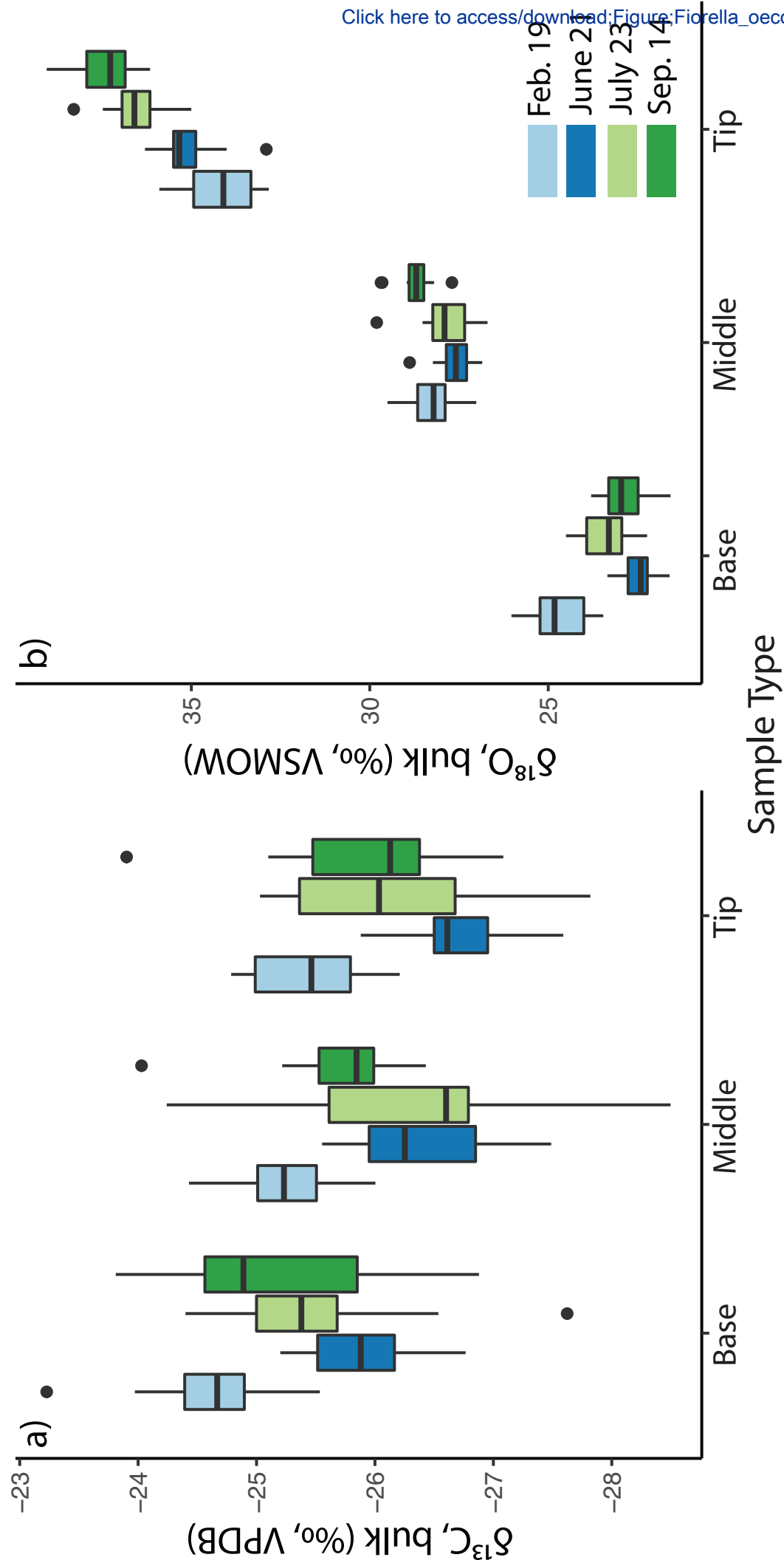
Fig. 1

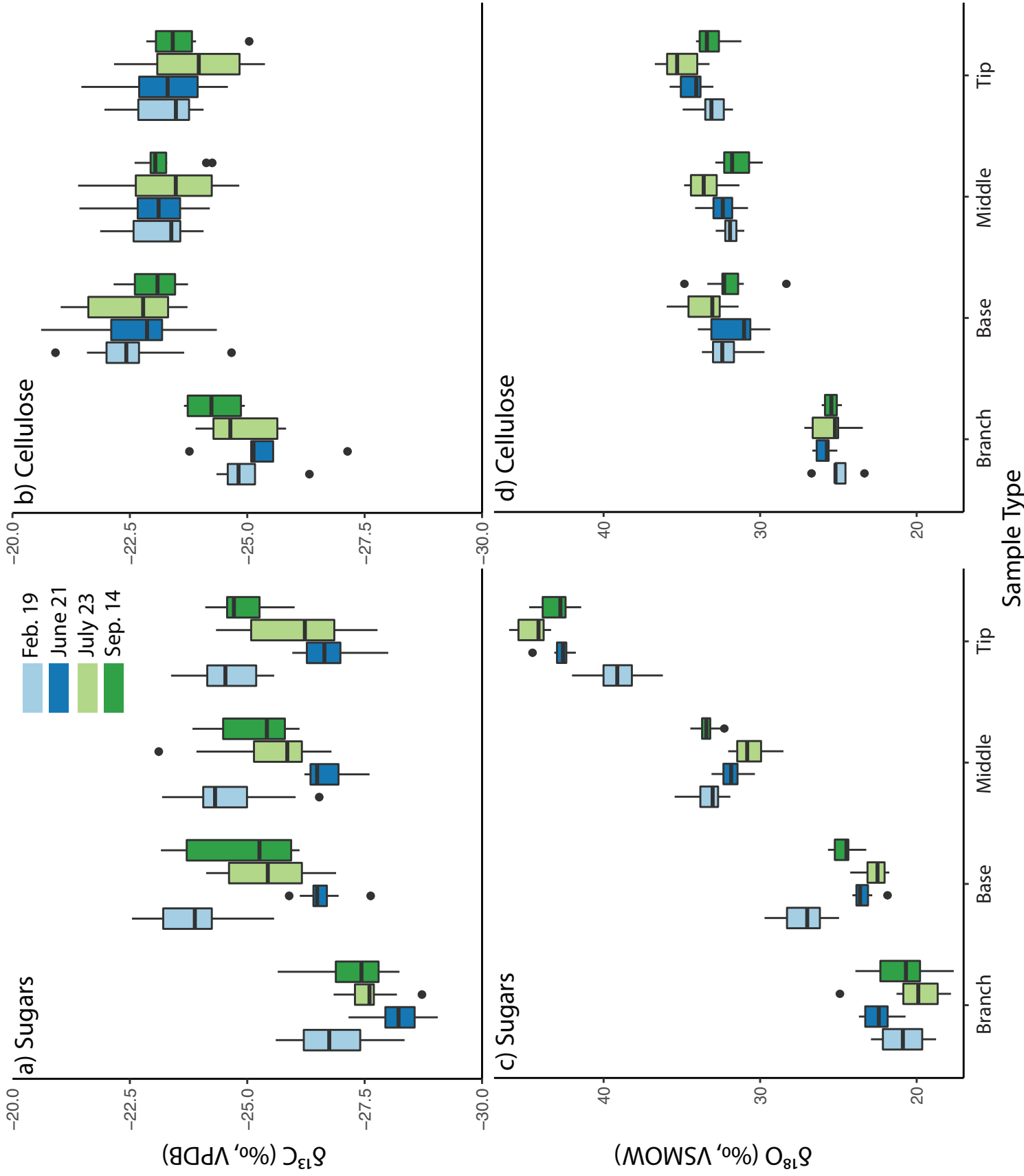
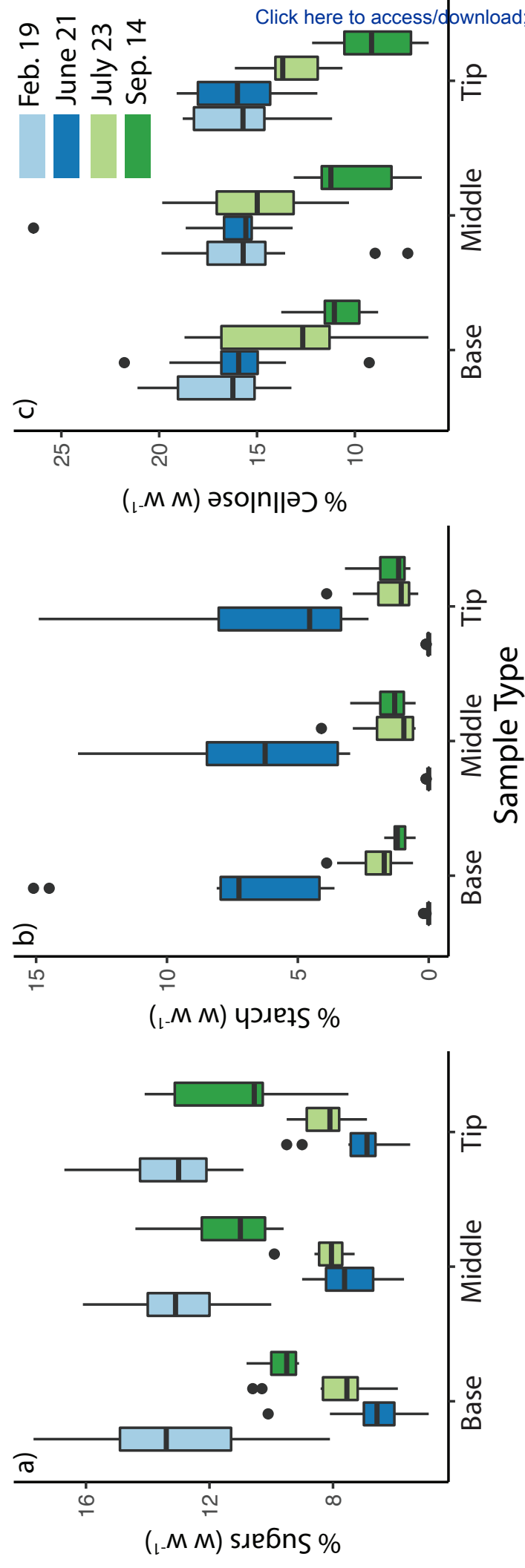
Fig. 2

Fig. 3



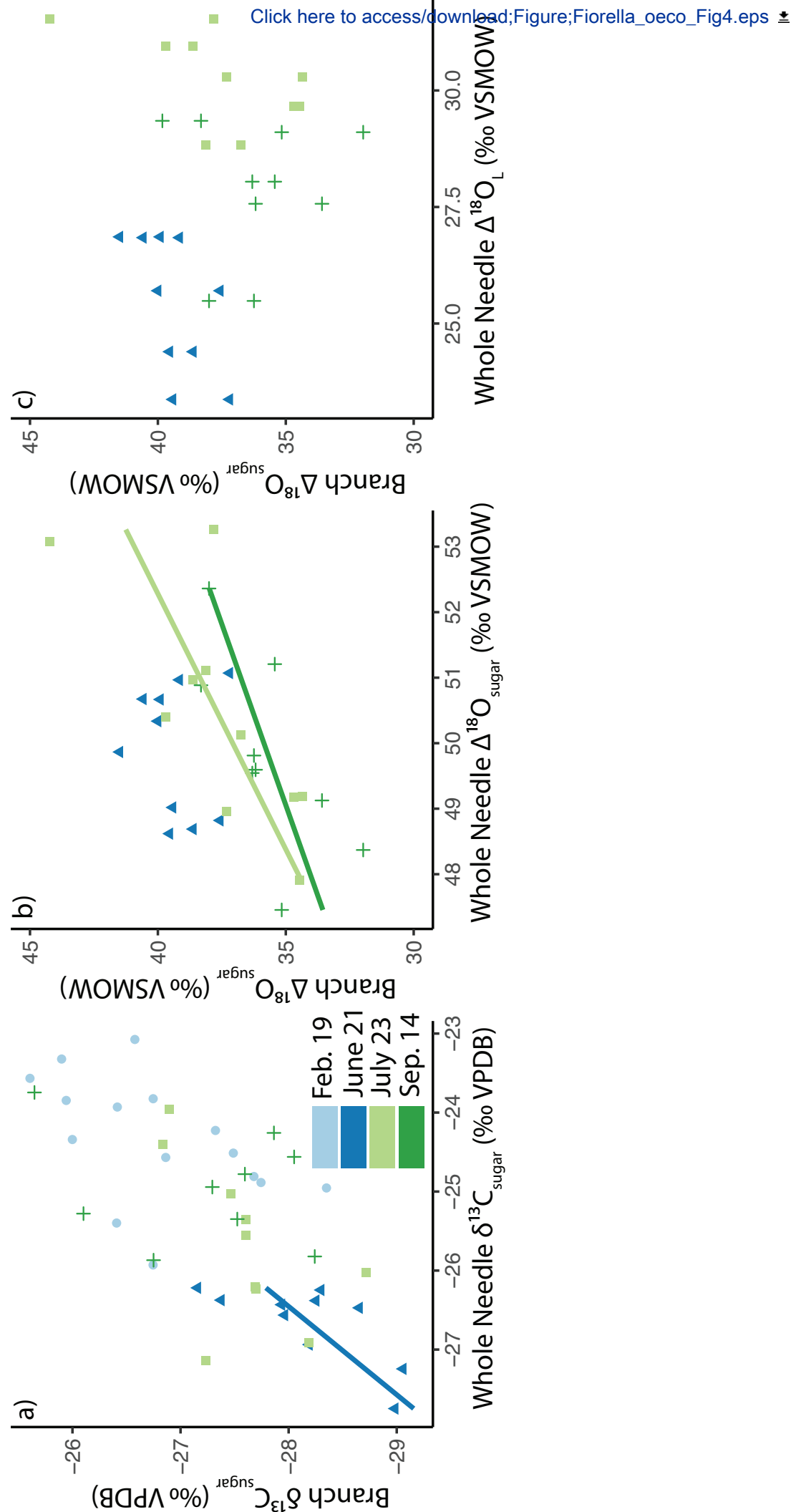


Fig. 5

